Two-magnon excitations in the Heisenberg ferromagnet on the triangular lattice

1992 J. Phys.: Condens. Matter 4 5419

(http://iopscience.iop.org/0953-8984/4/24/012)

J. Phys.: Condens. Matter 4 (1992) 5419–5432. Printed in the UK

Two-magnon excitations in the Heisenberg ferromagnet on the triangular lattice

X H Qu† and P D Loly

Department of Physics and Winnipeg Institute for Theoretical Physics, University of Manitoba, Winnipeg, Manitoba R3T 2N2, Canada

Received 13 December 1991, in final form 19 March 1992

Abstract. The spectrum of two-magnon excitations is examined for a 2D triangular Heisenberg ferromagnet with various values of spin (S), Ising (σ) and uniaxial (D) anisotropies and for total wavevectors K in three high-symmetry directions. In contrast to earlier studies of hypercubic ferromagnets (nearest neighbour (NN) chain, square and simple cubic), the width of the continuum never goes to zero, rather reminiscent of the NN FCC case, and the S, σ, D parameters are found to be very significant for the behaviour of s, d and single-ion bound states, as well as the continuum which was not probed in earlier studies. Internal van Hove singularities play an important role in the evolution of resonances within the continuum. Finally the results are compared with a Raman scattering experiment on $FeBr_2$.

1. Introduction

Bethe [1] first discovered the bound complexes of spin waves in the 1D Heisenberg ferromagnet. His work stimulated a general concern about the spectra of two interacting magnons in the Heisenberg model. Dyson [2] derived a weak T^4 correction as their temperature effect on the magnetization. Wortis [3] later recovered Bethe's results with a systematic Green's function formalism, and established the existence of two-magnon bound states in 2D and 3D isotropic hypercubic lattices. In 1D there is always one bound state for all pair wavevectors $K = k_1 + k_2$; in 2D at least one, with another at large K; and for 3D a large region around $K = 0$ with no bound states, but with one, two and three bound states at larger K. Extensions have been made by other workers, especially for the incorporation of uniaxial anisotropy [4, 5] and of biquadratic exchange [6, 7]. In 1D, Majumdar [8] made an early study on bound states in the presence of next-nearest neighbour (NNN) interaction in the late 1960s. In an important contribution Boyd and Callaway [9] showed that the doublet bound state broadened into a resonance inside the continuum.

Later Loly and Choudhury [10] extended the investigation of the evolution of the bound states and resonance modes and transitions between them for all K. The

† Present address: Department of Metallurgy and Material Science, University of Toronto, Toronto, Ontario M5S 1A4, Canada.

0953-8984/92/245419+14$04.50

relationship between continuum structure and the occurrence of bound states, the role of van Hove singularities in determining the positions of resonances, and interpretation of corresponding Raman scattering experiments (corresponding to the $K = 0$ continuum) has been reviewed by Loly [11]. The nearest neighbour (NN) simple-cubic (SC) Heisenberg model with various values of uniaxial anisotropy was studied in [12]. The NNN exchange interaction on the SC lattice was discussed in [13], where it was shown that large enough NNN exchange can actually prevent the formation of bound states. The NNN 1D chain and NN square lattice continua are investigated thoroughly in [14] and [15]. Although most information has been obtained for hypercubic lattices, the continuum structure has not been fully explored for the rather more complicated 2D triangular ferromagnet, as was the case earlier for the FCC case [16]. This has relevance to $FeBr_2$ [17] whose anti-ferromagnetically coupled ferromagnetic layers are modelled by our present 2D triangular study, and possibly also to nuclear magnetism in layers of ^3He on graphite [18]. Previous work by Wada, Ishikawa and Oguchi [19] studied the bound states in the isotropic triangular ferromagnet for spin $\frac{1}{2}$, and their numerical study of the bound state equations revealed bound states at large K. The weak binding energy of the s-wave bound state makes it difficult to follow it to small values of K in some numerical calculations, although analogy with the 2D square lattice [3] leads one to expect it to persist down to $K = 0$. Earlier Tonegawa [4] developed a formalism for the bound-state problem for $S \geqslant 1$ and he applied his bound-state results to the quasi-2D $FeCl_2$ ($S = 1$) which has a large enough single-ion anisotropy to form a bound state below the continuum at $K = 0$. However, neither study was able to probe the density of states inside the continuum. In this paper we employ the Green's function formalism, following the line of Wortis [3] and Loly *et al* [12, 13], to make a complete analysis of both bound states and the continuum resonances. Significant interplay between the resonances in the continuum and the bound states is then clearly revealed. The contribution of spin value (S), Ising anisotropy (σ) and single-ion anisotropy (D) is also fully studied.

A spin Green's function formalism is ideally suited to the thorough study of two-magnon excitations at absolute zero temperature because the equation of motion for the two-magnon propagator terminates without the need for any decoupling approximations, thereby yielding an exact set of simultaneous equations for the Green's functions of interest. This is soluble within controllable numerical precision if the range of exchange interactions is finite. The Green's function method can also be extended to a more complete analysis of the process in Raman scattering experiments. Unlike the Bethe *ansatz* [1] and real-space rescaling [20], which are really only useful in 1D, the Green's function method works in any dimension, leaving only the operation of evaluating the so-called lattice Green's functions (LGF).

Section 2 summarizes the necessary Green's function formulae and the Dyson equation for the two-magnon propagators at $T = 0$ K. It is then applied to the triangular ferromagnet in section 3. Critical points (van Hove-type singularities) for the non-interacting two-magnon problem are discussed in section 4. Section 5 discusses the results of extensive numerical computations for bound states and resonances in both isotropic and anisotropic situations. A comparison is made with the Raman scattering experiments on $FeBr_2$ [17] which has layers of triangular ferromagnetic sheets. The conclusions to be drawn from this study are then given in section 6.

2. The two-magnon propagator

The system we are considering is described by the Heisenberg Hamiltonian

$$H = -\sum_{ij}(I_{ij}S_i^zS_j^z + J_{ij}S_i^+S_j^-) - \sum_i D(S_i^z)^2 \tag{1}$$

where a total spin operator S_i is assigned to the atom on the ith lattice site. $I_{ij} = I(|R_i - R_j|)$ and $J_{ij} = J(|R_i - R_j|)$ denote the exchange integrals coupling the atoms on ith and jth lattice sites, which are a function of the relative distance between two sites. I_{ij} and J_{ij} denote the longitudinal and transverse terms, respectively. The limit $J_{ij} = 0$ gives the well known Ising model. D controls the uniaxial single-ion anisotropy.

The derivation of the two-magnon propagator at absolute zero closely follows those given in previous papers [12–14] and only a brief outline is presented here (a step-by-step derivation is displayed in [21]). The scattering of two magnons with initial wavevectors k_1, k_2 and final wavevectors k'_1, k'_2 is described by the Green's function,

$$\begin{aligned} G(k_1,k_2;k'_1,k'_2,t) &= -i\theta(t)\langle 0|[S^-_{k_1}(t)S^-_{k_2}(t), S^+_{k'_1}(0)S^+_{k'_2}(0)]|0\rangle \\ &= \langle\langle S^-_{k_1}(t)S^-_{k_2}(t)|S^+_{k'_1}(0)S^+_{k'_2}(0)\rangle\rangle. \end{aligned} \tag{2}$$

The equation of motion for the Green's function has the standard form

$$\omega G(k_1,k_2;k'_1,k'_2,\omega) = \langle 0|[S^-_{k_1}S^-_{k_2}, S^+_{k'_1}S^+_{k'_2}]|0\rangle + \langle\langle [S^-_{k_1}S^-_{k_2}, H]|S^+_{k'_1}S^+_{k'_2}\rangle\rangle_\omega. \tag{3}$$

Introducing a partial Fourier transformation,

$$G(i,j,K,\omega) = \frac{1}{N}\sum_{kk'} G(K,k,K,k',\omega)\exp(-ik\cdot R_i + ik'\cdot R_j) \tag{4}$$

where we define the total and relative wavevectors,

$$\begin{aligned} K &= k_1 + k_2 \qquad k = (k_1 - k_2)/2 \\ K' &= k'_1 + k'_2 \qquad k' = (k'_1 - k'_2)/2. \end{aligned} \tag{5}$$

Conservation of total wavevector should be maintained during the process of partial Fourier transformation, i.e. $K = K'$. It can then be shown that the equation of motion in (3) leads to the following Dyson's equation

$$\begin{aligned} G(i,j,K,\omega) = {} & 8S^2\left(1 - \frac{\delta_{j0}}{2S}\right)\Lambda(i,j,K,\omega) + 2\sum_l I_l\tilde{\Lambda}(i,l,K,\omega)G(l,j,K,\omega) \\ & + 2\sum_l (J_l - I_l)\left[\Lambda(i,l,K,\omega) + \tilde{\Lambda}(i,l,K,\omega)\right]G(l,j,K,\omega) \\ & - 2\sum_l D\Lambda(i,l,K,\omega)G(l,j,K,\omega)\delta_{l0} \end{aligned} \tag{6}$$

where

$$\Lambda(i,j,K,\omega) = \frac{1}{N}\sum_k \frac{\cos k\cdot R_i \cos k\cdot R_j}{\omega - \Omega(K,k)}$$

$$\tilde{\Lambda}(i,j,K,\omega) = \frac{1}{N}\sum_k \frac{\cos k\cdot R_i(\cos\tfrac{1}{2}K\cdot R_j - \cos k\cdot R_j)}{\omega - \Omega(K,k)}$$

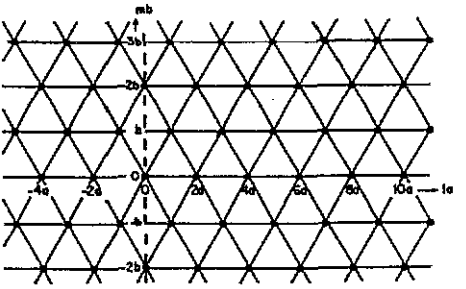

Figure 1. The real-space network of the triangular lattice.

in which $\Omega(K,k)$ is the total energy of a non-interacting two-magnon state

$$\Omega(K,k) = 2S[2I(0) - J(\tfrac{1}{2}K + k) - J(\tfrac{1}{2}K - k)] + 2(2S-1)D \quad (7)$$

and

$$J(k) = \sum_l \exp^{ik\cdot R_l} J(R_l) \quad (8)$$

and similarly for $I(0)$.

Dyson's equation can be further expressed in terms of LGF as

$$G(i,j,K,\omega) = 4S^2\left(L_{i-j} + L_{i+j} - \frac{1}{S}L_i\delta_{j0}\right) - 2\sum_l I(l)L_{l-i}G(l,j,,K,\omega)$$
$$+ 2\sum_l J(l)\cos(\tfrac{1}{2}K\cdot R_l)L_iG(l,j,K,\omega) - 2DL_iG(0,j,K,\omega). \quad (9)$$

The LGFs are defined by

$$L_i(K,\omega) = \frac{1}{N}\sum_k \frac{e^{ik\cdot R_i}}{\omega - \Omega(K,k)}.$$

Dyson's equation is exact and valid for any lattice with an arbitrary range of interaction. However, one usually considers a certain approximations on the range of interaction so that the chain equations can be truncated to a finite set of equations.

3. Specializing to the triangular lattice

The Green's function $G(i,i,K,\omega)$ represents the propagator of a two-magnon process involving the creation of two spin deviations on two sites separated by a distance R_i (on a 2D lattice it is specified by two indices $R_i = (i_x, i_y)$). The spectral function of such a process is proportional to $-\operatorname{Im} G(i,i,K,\omega)$. In a two-dimensional triangular lattice (figure 1) we should specify the lattice site by

$$R_i = la + mb$$

where $l+m$ is an even integer, and a and b are equal to $\frac{1}{2}$ and $\frac{1}{2}\sqrt{3}$ of the edge of the basic cell of a triangular lattice.

In this work we will examine the spectra of single-ion two-spin deviations ($R_0 = (0,0)$) and also the NN deviations along the three different directions, which are $i = (2,0)$, $i = (1,1)$ and $i = (-1,1)$. Shorthand notations for these sites, $i = 0, 1, 1'$ and $1''$, are used respectively. These spectra are in turn represented by four Green's functions $G(0,0), G(1,1), G(1',1')$ and $G(1'',1'')$, respectively.

Considering only nearest-interactions (let $I_{ij} = I$, $J_{ij} = J$, and introduce an Ising parameter $\sigma = J/I$) the two-magnon dispersion function (7) for the triangular lattice is given by

$$\begin{aligned}\Omega(\boldsymbol{K},k) &= 8SI[3 - \sigma(2\alpha^2 - 1)\cos 2k_x a - 2\sigma\alpha\beta\cos k_x a\cos k_y b \\ &\quad - 2\sigma\sqrt{(1-\alpha^2)(1-\beta^2)}\sin k_x a\,\sin k_y b + 2(2S-1)D] \\ &= 8SI[3 - \sigma A\cos 2k_x a - 2\sigma B\cos k_x a\cos k_y b - 2\sigma C\sin k_x a\sin k_y b] \\ &\quad + 2(2S-1)D \qquad (10)\end{aligned}$$

where $\alpha = \cos\frac{1}{2}K_x a$, $\beta = \cos\frac{1}{2}K_y b$ and other parameters are defined as

$$A = 2\alpha^2 - 1 \qquad B = \alpha\cdot\beta \qquad C = \sqrt{(1-\alpha^2)(1-\beta^2)}.$$

The LGFs are expressed as the integrals over the Brillouin zone. The integrations are computed for general $\boldsymbol{K}$ using the linear analytical triangular method [22]. Some interesting recurrence relations of the lattice Green's functions for a general $\boldsymbol{K} \neq 0$ can be developed and these provide a way to check the results of numerical calculation [21]. Analytical expressions are available in some special cases. When $\boldsymbol{K} = 0$, Horiguchi [22] showed that the LGFs may be expressed in terms of the complete elliptic integrals of the first, second and third kind. Also at the M point, where $K_x = 0$ and $K_y = \pi$, the LGFs may be expressed in a rather simple form and evaluated even more easily [21].

With nearest-neighbour (NN) interactions, and taking into account some symmetry properties of the triangular lattice, it can be seen that (9) connects the four Green's functions mentioned above with each of the other three Green's functions. Letting i and j in Green's functions $G(i,j,\boldsymbol{K},\omega)$ take one of the four values $(0,0)$, $(2,0)$, $(1,1)$, and $(-1,1)$, and denoting $G(i,j,\boldsymbol{K},\omega)$ by the 4×4 matrix $\mathbf{G}$, the equations can be written more compactly as one matrix equation

$$(\mathbf{I} + \mathbf{Q})\mathbf{G} = \mathbf{R} \qquad (11)$$

where $\mathbf{I}$ is the identity matrix, the coefficient matrix $\mathbf{Q}$ is a 4×4 matrix, and another 4×4 matrix $\mathbf{R}$ contains all inhomogeneous terms. The elements of both $\mathbf{Q}$ and $\mathbf{R}$ are functions of the LGF. Solving this matrix equation will give the four diagonal spectra which interest us.

4. Critical points

Critical points are also important in analysing the structure of two-magnon propagators and their evolution as a function of $\boldsymbol{K}$. We define the density of states, or spectral function, of any excitation by

$$\rho(\omega) = \frac{1}{N}\sum_{k}\delta(\omega - \omega_k).$$

Here, k is the wavevector , and ω_k is the dispersion relation. Replacing the summation by an integration over the first BZ,

$$\rho(\omega) = \frac{V}{(2\pi)^3} \int_\omega \frac{ds}{|\nabla \omega_k|}.$$

The critical points occur when $|\nabla \omega_k| = 0$, and lead to the various singularities in the density of states. They were first studied by van Hove [24] in the context of one-particle excitations. Critical points are also important in analysing the structure of two-magnon propagators and their evolution as a function of K.

Differentiating (10) with respect to $k_x a$ and $k_y b$, with some simple algebra, we obtain the following solutions for critical points which can be divided into two groups. The first group is given by $\sin k_x a = \sin k_y b = 0$, or $\cos k_x a = \cos k_y b = 0$, for all values of α and β. They correspond to the high-symmetry points Γ (the centre of first BZ) and M, M', M'' of the first Brillouin zone in k space. They have energies,

$$\omega_\Gamma = 8SI\{3 - \sigma(2\alpha^2 - 1) - 2\sigma\alpha\beta\} + 2(2S-1)D \qquad \Gamma(k_x a = 0,\ k_y b = 0)$$

$$\omega_M = 8SI\{3 - \sigma(2\alpha^2 - 1) + 2\sigma\alpha\beta\} + 2(2S-1)D \qquad M(k_x a = 0,\ k_y b = \pi)$$

$$\omega_{M'} = 8SI\{3 + \sigma(2\alpha^2 - 1) - 2\sigma\sqrt{(1-\alpha^2)(1-\beta^2)}\} + 2(2S-1)D$$
$$M'(\pi/2, \pi/2)$$

$$\omega_{M''} = 8SI\{3 + \sigma(2\alpha^2 - 1) + 2\sigma\sqrt{(1-\alpha^2)(1-\beta^2)}\} + 2(2S-1)D$$
$$M''(-\pi/2, \pi/2).$$

In contrast to these four solutions the remaining group of critical points move in k space as α and β vary. They are determined by the set of equations:

$$2AB \cos k_x a = (C^2 - B^2) \cos k_y b$$

$$2AC \sin k_x a = (C^2 - B^2) \sin k_y b.$$

Some different cases of parameters B and C should be distinguished and treated separately. The full lines in figure 2 shows the critical lines of the isotropic 2D triangular lattice. (Ignore the other data for the moment.)

Loly *et al* have studied the dispersion of the critical points with K in the square lattice [15] and SC lattice [25]. With only isotropic NN interactions present, their critical points both consist of straightlines (if plotted as a function of α), which correspond to high-symmetry points Γ, X, M (and R in 3D SC), and both cases have zero bandwidth at the Brillouin zone corner. For the SC lattice these lines begin to bend, and critical lines which do not correspond to the high-symmetry points appear, only after the next-nearest-neighbour (NNN) coupling is taken into account. However, in the triangular lattice the complicated nature of the lattice results in both groups of critical lines bending, as well as a non-zero minimum bandwidth existing even when only NN isotropic interactions are present. A similiar phenomenon was also found for the NN FCC magnet [16].

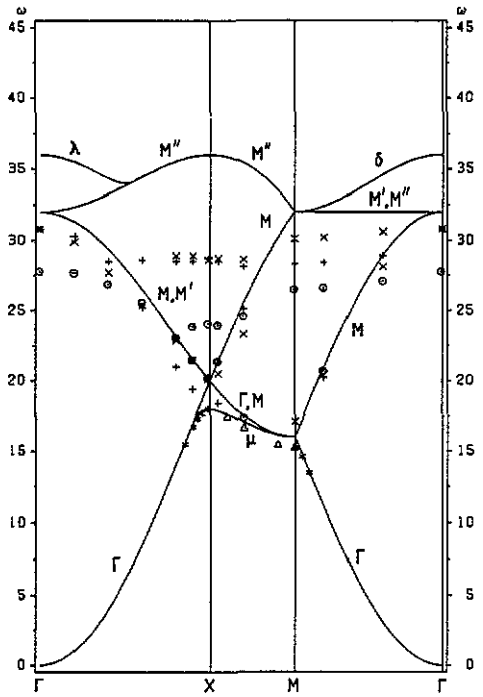

Figure 2. Dispersion of resonance peaks and bound states in the isotropic case; $D = 0$, $\sigma = 1$ and $S = 1$. The full curves give the upper and lower edges of the two-magnon continuum as well as the internal critical lines (labelled as Γ, M, M', M'', and λ, μ, δ), for ω as a function of K where K goes through $\Gamma \longrightarrow X \longrightarrow M \longrightarrow \Gamma$. The resonances of the three spectra are denoted by $\odot$ for $G(0,0)$, $+$ for $G(1,1)$, and $\times$ for $G(1',1')$. The bound states below the continuum are denoted by asterisks (*) for type-s, by triangles (Δ) for type-d.

5. Results and discussions

The main computational effort is associated with the evaluation and storage of the 10 LGFs for different K and ω values. The set of equations in (11) are then solved by numerically inverting $(\mathbf{I} + \mathbf{Q})$ and the diagonal Green's functions $G(0,0)$, $G(1,1)$, $G(1',1')$ and $G(1'',1'')$ are obtained. As K changes along high-symmetry directions from $\Gamma \longrightarrow X \longrightarrow M \longrightarrow \Gamma$, two of the three NN Green's functions are always identical, leaving only two of them independent. Therefore only $G(0,0)$, $G(1,1)$, $G(1',1')$ need to be presented here.

5.1. $S = 1$, $K = 0$ isotropic exchange

Figure 3 shows the continuum spectrum of $G(0,0)$, $G(1,1)$ in the isotropic case where $D = 0$, and $\sigma = 1$ for $K = 0$, and $S = 1$. With the unit of energy (ω) chosen as I, the peak of $G(0,0)$ is found at $\omega = 27.8$, while the peak of $G(1,1)$ is at $\omega = 30.8$. The critical point at $\omega = 32.0$ is associated with a sharp drop in both $G(0,0)$ and $G(1,1)$ and creates a shoulder above this point. At $K = 0$ the rise in $G(1,1)$ at the bottom of the band is all that remains of the s-wave exchange bound state, whose binding energy vanishes at that point.

In previous studies [11] it has been instructive to locate the Ising levels, which are obtained by reducing J_{ij} (the transverse terms of the exchange integrals in (1)) to zero. In this limit, the energy of two spin deviations on adjacent lattice sites (NN) is $22SI + 2D(2S - 1)$, while two deviations on the same site (single-ion) require an energy of $24SI$.

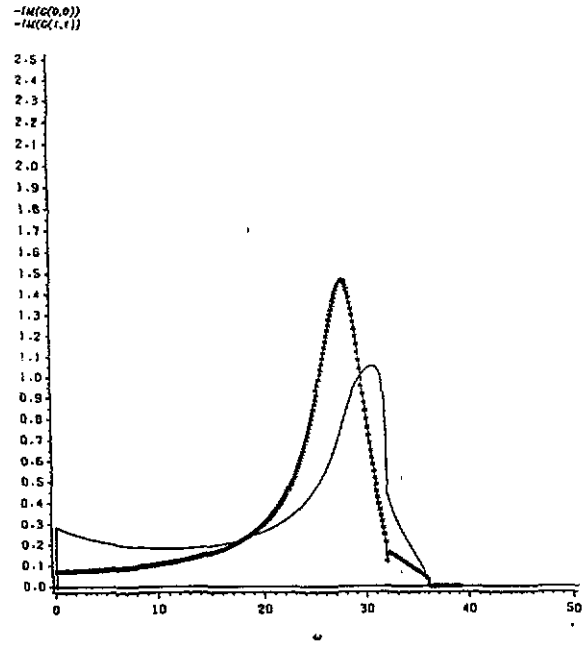

Figure 3. Two-magnon spectra at $K = 0$ in the isotropic case; $D = 0$, $\sigma = 1$ and $S = 1$. The asterisked curve represents single-ion spectra, $-\operatorname{Im} G(0,0)$, while the full curve represents NN spectra, $-\operatorname{Im} G(1,1)$.

5.2. $S = 1$, $K \neq 0$ isotropic exchange

In our numerical calculations we begin to detect bound states below the lower boundary of the continuum as K moves close to X, the corner of the first BZ. For $K \neq 0$ the excitations along different directions are certainly different so that the degeneracy at $K = 0$ is lifted by the appearance of a second distinct NN excitation spectrum, $G(1',1')$. As $|K|$ increases, the principal resonances of single-ion spectra and the two nearest-neighbour spectra generally move down in energy. Figure 2 shows how the resonances of the continuum and the bound states evolve as a function of K in the isotropic case. In our Green's function formalism the bound state is expressed by a δ-function singularity of the imaginary part of the Green's function located outside the boundaries of the continuum. The real part of the Green's function exhibits x^{-1}-type behaviour at points where the imaginary part exhibits a δ-function singularity. Since a δ-function in the spectra of $\operatorname{Im} G(i,i,K,\omega)$ is too narrow to be detected, in practice the bound state is located by checking the sign change of $\operatorname{Re} G(i,i,K,\omega)$. In the isotropic case our numerical calculations only resolve one bound state below the continuum for $S = 1$. It keeps very close to the bottom of the continuum, and appears to join the continuum at the X point ($K = (\frac{1}{3}\pi, \pi)$), but is found again in the X $\longrightarrow$ M region. These bound states are identified as poles of all three two-magnon propagators $G(0,0)$, $G(1,1)$, $G(1',1')$ in the $\Gamma \longrightarrow$ X region and also in the M $\longrightarrow \Gamma$ region, but they are the poles of the propagator $G(1',1')$ only in the X $\longrightarrow$ M region. We adopt the commonly used terminology of the hypercubic case [12] to call the bound state where all three Green's functions have poles the 'type-s' exchange bound state, and the bound state where only $G(1',1')$ has pole 'type-d'. In the absence of anisotropy our numerical results for $S = 1$ resolve only the type-s

bound state in the $\Gamma \longrightarrow X$ and $M \longrightarrow \Gamma$ regions, and only the type-d bound state in the $X \longrightarrow M$ region.

5.3. Resonance dynamics and the continuum structure

The critical lines exhibit a very strong influence on evolution of the spectrum. In figure 2, the $G(1,1)$ and $G(1',1')$ resonances approach the critical line M, M' between 0.40 and 0.60 ($\Gamma \longrightarrow X$). (Here we introduce notation for positions along the line from Γ to X.) While the principal peak is restrained below the critical line, an additional hump shows up on the upper side of the critical line. Such effects were first observed by Loly and Choudhury [10] in a study of the NN SC case. The same phenomenon is also detected in the $G(0,0)$ resonance when it reaches the critical line between 0.80 and 0.90 ($\Gamma \longrightarrow X$). The principal resonances of neither $G(0,0)$, nor $G(1,1)$, nor $G(1',1')$ appear to be able to penetrate the critical line. However, $G(1,1)$ shows a stronger repulsion with the critical line, such that it crosses over both $G(0,0)$ and $G(1',1')$ on the way to the zone corner. In the ($X \longrightarrow M$) region, some weight builds up along the line M' (figure 2) and joins with the upper humps which just penetrate the M'-line. Other peaks pick up from the bottom at $K = (0,\pi)$ (M-point) and climb along the line M. Eventually all peaks join together as K goes back to Γ—our starting point at the centre of the first BZ. Figure 4 shows the spectrum of two-magnon propagators of an isotropic lattice for some selected K values, which forms the basis for figure 2. In particular, figure 2(*a*) shows very strong enhancement at the bottom of the band for $G(0,0)$, $G(1,1)$ and $G(1',1')$ at the point $K = 0.8$ ($\Gamma \longrightarrow X$). This is associated with the type-s bound state, which lies just below the bottom edge near X. The influence in the continuum of bound states is more visibly illustrated in the $X \longrightarrow M$ region, where sharp peaks very close to the bottom of the continuum are found at $K = 0.1$ ($X \longrightarrow M$) in both the $G(1,1)$ and $G(1',1')$ spectra. The type-d bound state, which is the pole of $G(1',1')$, is then close to the edge. At $K = 0.4$ ($X \longrightarrow M$) only a strong enhancement of $G(1,1)$ is detected at the bottom of continuum, while the weight of $G(1',1')$ probably goes into this bound state.

5.4. Spin dependence

The effect of the spin magnitude S, which is often ignored by previous researchers, is found to be quite significant to the behaviour of bound states, as shown in figure 5. For $S = 1$ our numerical results find only one bound state at each K value. When the value of S changes from 1 to 1/2, while other parameters are kept the same, the bound states are more strongly bound so that when $S = 1/2$ we find both type-s and type-d bound states for large $|K|$ values in the neighbourhood of the X point. Our results are consistent with the $S = 1/2$ results of Wada *et al* [19], but unfortunately they did no calculations for $S = 1$.

Wada *et al* [19] have examined the bound states of the 2D triangular lattice for $S = \frac{1}{2}$ by another method, which is described in Mattis's book [26]. In order to compare with our results, we programmed their formulae, recalculated the bound states at both $S = 1$ and $S = \frac{1}{2}$, and carefully compared the data from the two methods. All results reached full agreement within the resolution of their published diagrams.

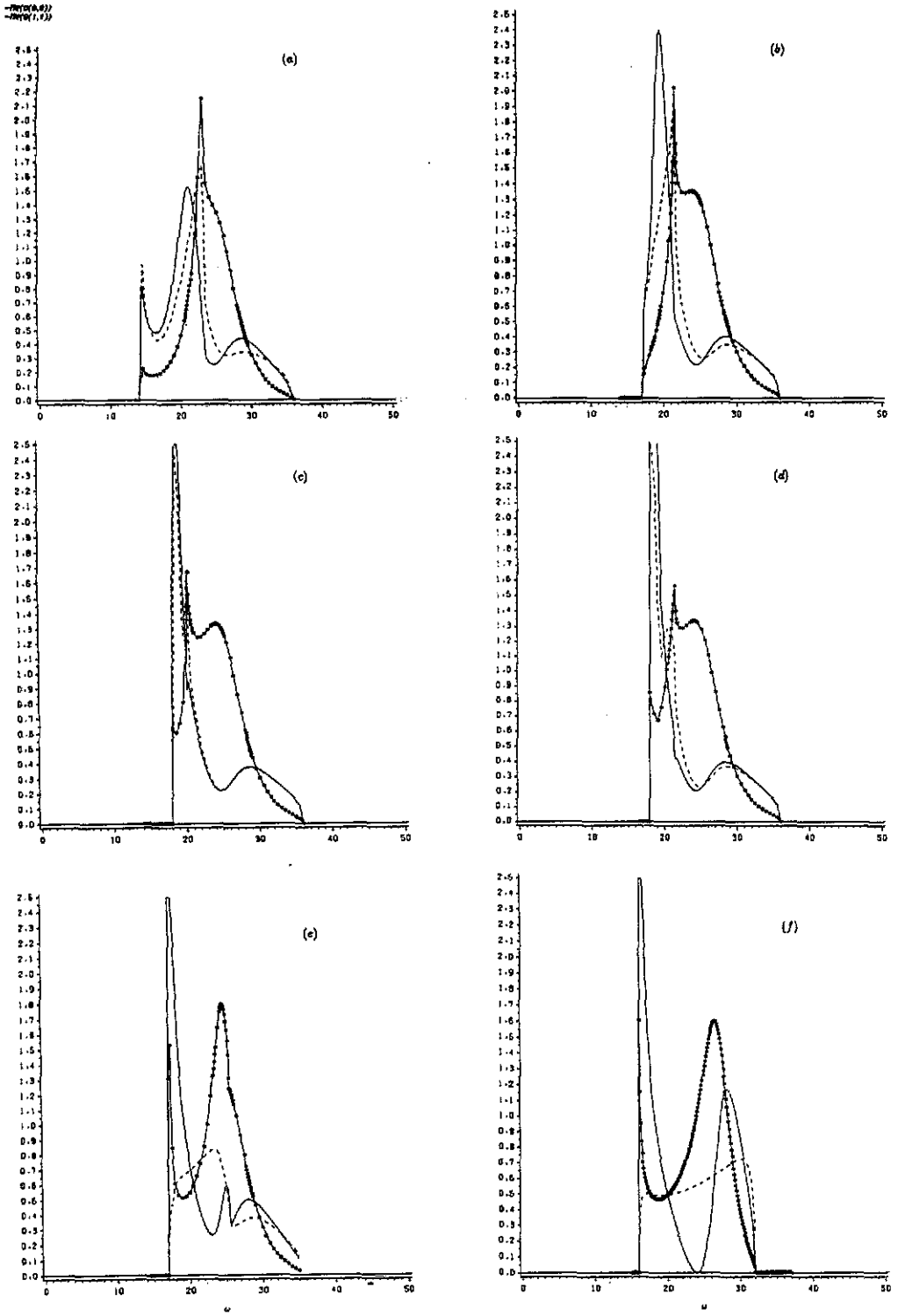

Figure 4. Two-magnon spectra of selected value of K as a function of ω. The cases shown are (*a*) $K = 0.8$, along Γ–X, (*b*) $K = 0.9$, along Γ–X, (*c*) X point, (*d*) $K = 0.1$, along X–M, (*e*) $K = 0.4$, along X–M, (*f*) M point. The graphs all concern the case of $S = 1$ and isotropic exchange. In all cases the asterisked curve is used for $G(0,0)$, a full curve for $G(1,1)$, and a broken curve for $G(1',1')$.

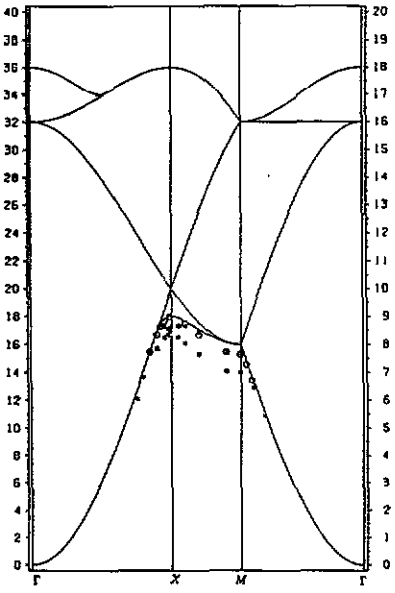

Figure 5. Comparison between the bound states of $S = 1$ and $S = \frac{1}{2}$ in the isotropic case, as K goes through $\Gamma \longrightarrow X \longrightarrow M \longrightarrow \Gamma$. The critical-point singularities are labelled as in figure 3. For reference the energy (unit, I) is scaled for $S = 1$ at the left, and for $S = 1/2$ at the right. The bound states below the continuum are denoted by ⊙ for $S = 1$ and by asterisks for $S = 1/2$. For clarity, the type-s and type-d are labelled by the same symbol.

5.5. Anisotropies

We studied several different cases of anisotropies by experimenting with the size of the D and σ anisotropies respectively. For a brief illustration we only present one case where D and σ are taken as 2.26 and 0.78, respectively. These particular values are chosen to compare with the Raman scattering experiment which is discussed in the next subsection. D anisotropy produces a gap below the continuum band and lifts the whole band by $2(2S-1)D$, while σ anisotropy squeezes the band. Figure 6 shows the spectrum at the BZ centre ($K = 0$). In general, the resonance of $G(0,0)$ at $K = 0$ is barely affected when D introduces the shift, but it is affected slightly when σ deforms the continuum. On the other hand, the resonance of $G(1,1)$ exhibits significant changes when various D and σ are introduced. However, the position of the resonance with respect to the band remains essentially unchanged. Figure 7 shows the critical lines still playing an important role in directing the evolution of resonances, as is also shown in our discussion of the isotropic case. However, there are some significant differences due to the effect of anisotropies. The trajectories of the resonances are apparently shifted, mainly due to the shift of their starting points, as we discussed in the previous paragraph. Another phenomenon is that the humps formed on the upper side of the critical line become much smaller as D becomes larger. From several different anisotropic cases which we have studied [11], it appears that the evolution of resonances can probably be determined roughly by knowing their starting positions and the topology of the critical lines.

The positions of type-s and type-d bound states are barely changed by the presence of D and σ, though our study of other anisotropic cases shows that they seem to be 'pulled' slightly closer to the bottom of the continuum by the single-ion anisotropy (D). The formation of additional 'single-ion' bound states is detected as expected, enhanced by the effect of the D anisotropy. For relatively small values of D, we used a hybridization of type-s with the single-ion type of bound states that exist for all regions $\Gamma \longrightarrow X \longrightarrow M \longrightarrow \Gamma$. For much larger values of single-ion anisotropy a

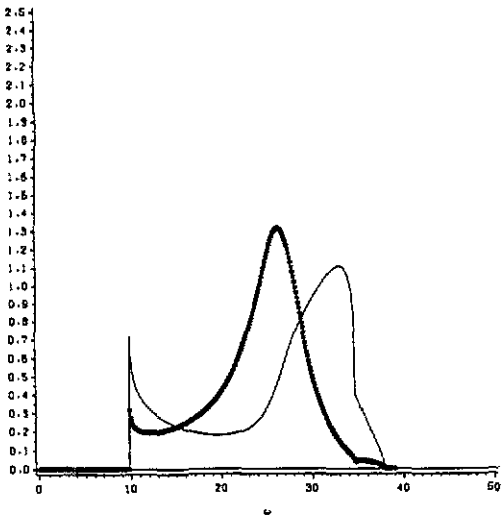

Figure 6. Two-magnon spectra at $K = 0$ for $D = 2.26, \sigma = 0.78$ and $S = 1$. The asterisked curve represents single-ion spectra, $-\operatorname{Im} G(0,0)$, the full curve represents NN spectra, $-\operatorname{Im} G(1,1)$.

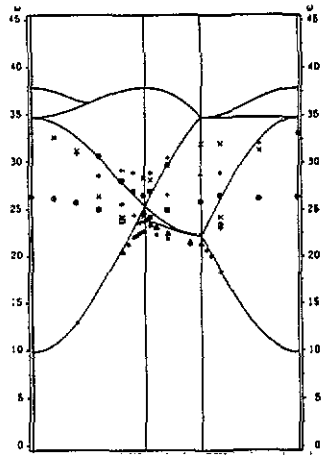

Figure 7. Dispersion of resonance peaks and bound states for $D = 2.26, \sigma = 0.78$ and $S = 1$, as K goes through $\Gamma \longrightarrow X \longrightarrow M \longrightarrow \Gamma$. The critical-point singularities are denoted with the same convention as in figure 3. The resonances of the three spectra are denoted by $\odot$ for $G(0,0)$, + for $G(1,1)$, and x for $G(1',1')$. The bound states below the continuum are denoted by asterisks for type-s, and triangles for type-d. The 'single-ion' bound state which lies below both type-s and type-d is also denoted by an asterisk.

true single-ion bound state will be found to extend to the BZ centre ($K = 0$).

5.6. A 2D model for $FeBr_2$ and Raman scattering

Two-magnon Raman scattering was discovered in the mid-1960s when lasers became available for studying solids [27]. For transparent antiferromagnets, Fleury [28] showed that the strong magnon–magnon interactions distorted the spectra from the bare density of states; this was soon explained by the theoretical calculation of Elliott *et al* [29]. The small wavevector of optical radiation means that one-magnon scattering occurs in the centre region of the Brillouin zone ($K = 0$); the two-magnon process arises from a pair of magnons with equal and opposite wavevectors, so that again the total wavevector (K) is constrained to the centre of the first Brillouin zone.

Raman scattering in $FeBr_2$ has been studied by Psaltakis *et al* [17] and Johnstone *et al* [30]. The structure of $FeBr_2$ comprises layers of cations sandwiched between two layers of anions, with such composite sheets stacked along the trigonal c axis. The Fe^{2+} layer is a two-dimensional triangular lattice. This salt is known to exhibit certain two-dimensional ferromagnetic character below the Néel temperature, since the inter-sublattice coupling is substantially smaller than the intra-sublattice coupling. Psaltakis *et al* [17] identified the peak at 90.6 $cm^{-1} = 27.96I$ as a two-magnon line,

and interpreted the two peaks at 29.6 $cm^{-1} = 9.14I$ and 127.5 $cm^{-1} = 39.35I$ as possible evidence of two-magnon bound states below and above the continuum, respectively. In our calculation, where $D = 2.27$ and $\sigma = 0.78$ are chosen to reflect the parameters measured in the $FeBr_2$ salt, we found the resonance of $G(0,0)$ at $26.4I$ and $G(1,1)$ at $33.10I$, while lower and upper boundaries of the continuum are at $9.77I$ and $37.8I$, respectively. This is in reasonable agreement with the experiment of Psaltakis *et al*, even though our model only consists of a single layer of the triangular lattice and nearest-neighbour interactions. Further study incorporating three-dimensionality is needed in order to to give a more precise explanation of the shape of the Raman spectrum. Such calculations would, at present, be quite formidable computationally.

In $FeBr_2$ the ratio of the NN interlayer coupling parameter to the NN intralayer parameter is 0.29. The same ratio in $FeCl_2$, which has similiar magnetic structure, is only 0.05 [31]. In this sense $FeCl_2$ seems even closer to our 2D triangular model. However the two-magnon scattering peak in $FeCl_2$ was not found experimentally [31], and we expect, following Tonegawa [4], that a single-ion bound state below the continuum would be a strong feature of its strong uniaxial anisotropy.

6. Conclusions

The behaviour of two-magnon bound states and resonances of the 2D NN triangular Heisenberg ferromagnet was examined for total pair wavevectors K in three high-symmetry directions. The general results are found to be consistent with the previous work in the 3D lattice, as well as the plane square lattice. However, the more complicated nature of the triangular lattice does give rise to some interesting phenomena which are not present in simpler lattice structures. The effect of the spin magnitude S, which is rarely considered by other researchers, is found to be quite significant. The NN triangular case shares with the NN FCC case a non-zero minimum width of the continuum (as plotted as a function of K). It also has a much more complicated internal structure of the non-interacting spectrum as shown by our study of its critical lines. A strong enough D always produces a single-ion bound state, while a small enough σ also helps form bound states.

The general trends which we have elucidated give a reasonable degree of confidence that the simpler analysis of the unperturbed continuum structure would enable one to predict the behaviour of the resonances once a starting point has been established. We have compared our results with the available data from Raman scattering experiments for $FeBr_2$ and a fairly good agreement is achieved.

Acknowledgments

We thank B W Southern, D J Lockwood and M G Cottam for helpful discussions. This research was supported in part by a research grant from the Natural Sciences and Engineering Research Council of Canada through grant OGP0005036 to P D Loly, and in part by a graduate fellowship from the University of Manitoba to X H Qu.

Note added in proof. We agree with an observation by one of the referees that it is expected that a bound state exists for all K, in analogy with the NN square lattice [26]. This follows from the finite band edge density-of-states of bare magnons (and hence LGF) characteristic of 2D lattices for all K except at the M point (where these singularities become inverse square roots through collapse to 1D). Numerical calculations of the type used here are not optimized to search for very weakly bound states, but rather address the question of continuum structure in general in order to gain an understanding of the location of two-magnon Raman resonances.

References

[1] Bethe H 1931 *Z. Phys.* **71** 205
[2] Dyson F J 1956 *Phys. Rev.* **102** 1217, 1230
[3] Wortis M 1963 *Phys. Rev.* **132** 85
[4] Tonegawa T 1970 *Suppl. Prog. Theor. Phys.* **46** 61–83
[5] Silberglitt R and Torrance J B 1970 *Phys. Rev.* B **2** 772
[6] Pink D and Tremblay P 1974 *Can. J. Phys.* **50** 33
[7] Chiu-Tsao S T, Levy P M and Paulson C 1975 *Phys. Rev.* B **12** 1819
[8] Majumdar C J 1969 *J. Math. Phys.* **10** 177–80
[9] Boyd R G and Callaway J 1965 *Phys. Rev.* A **138** 1621
[10] Loly P D and Choudhury B J 1976 *Phys. Rev.* B **13** 4019–28
[11] Loly P D 1987 *Can. J. Phys.* **65** 1272–9
[12] Bahurmuz A A and Loly P D 1980 *Phys. Rev.* B **22** 1294–9
[13] Bahurmuz A A and Loly P D 1980 *Phys. Rev.* **21** 1924–9
[14] Bahurmuz A A and Loly P D 1986 *J. Phys. C: Solid State Phys.* **19** 2241–52
[15] Hood M and Loly P D 1986 *J. Phys. C: Solid State Phys.* **19** 4729–40
[16] Bahurmuz A A and Loly P D 1987 *J. Phys. C: Solid State Phys.* **20** 6277–85
[17] Psaltakis G C, Mischler G, Lockwood D J, Cottam M G, Zwick A and Legrand S 1984 *J. Phys. C: Solid State Phys.* **17** 1735–52
[18] Elser V 1989 *Phys. Rev. Lett.* **62** 2405–8
[19] Wada K, Ishikawa T and Oguchi T 1975 *Prog. Theor. Phys.* **54** 1589–98
[20] Southern B W and Liu T S 1989 *Phys. Rev.* **39** 160–4
[21] Qu Xiaohua 1989 Two-magnon excitations in the Heisenberg ferromagnet on the triangular lattice *MSc Thesis* University of Manitoba, Winnipeg, Canada
[22] Ashraff J A and Loly P D 1987 *J. Phys. C: Solid State Phys.* **20** 4823–31
[23] Horiguchi T 1972 *J. Math. Phys.* **13** 1411
[24] van Hove L 1953 *Phys. Rev.* **89** 1189–93
[25] Bahurmuz A A and Loly P D 1979 *Phys. Rev.* B **19** 5803–9
[26] Mattis D C 1965 *Theory of Magnetism* 1st edn (New York: Harper and Row) p 145
[27] Halley J W and Silvera I 1965 *Phys. Rev. Lett.* **15** 654
[28] Fleury P A 1968 *Phys. Rev. Lett.* **21** 151
[29] Elliott R J, Thorpe M F, Imbusch G F, Loudon R and Parkinson J B 1968 *Phys. Rev. Lett.* **21** 147
[30] Johnstone I W, Lockwood D J and Mischler G 1978 *J. Phys. C: Solid State Phys.* **11** 2147–64
[31] Lockwood D J, Mischler G, Zwick A, Johnstone I W, Psaltakis G C, Cottam M G, Legrand S and Leotin J 1982 *J. Phys. C: Solid State Phys.* **15** 2973–92